

High Speed Nanotechnology-Based Photodetector

Russell M. Kurtz, Ranjit D. Pradhan, Alexander V. Parfenov, Jason Holmstedt, Vladimir Esterkin,
Naresh Menon, Tin M. Aye, and Kang-Bin Chua
Physical Optics Corporation, Electro-Optics and Holography Division,
20600 Gramercy Blvd. Bldg. 100, Torrance, CA 90501

Axel Schindler
University of Stuttgart, Stuttgart, Germany

Alexander A. Balandin
Nano-Device Laboratory, University of California
Riverside, CA 92521

James E. Nichter
Air Force Research Laboratory, Photonics Processing Branch (SNDP),
25 Electronic Parkway, Rome, NY 13441

ABSTRACT

An inexpensive, easily integrated, 40 Gbps photoreceiver operating in the communications band would revolutionize the telecommunications industry. While generation of 40 Gbps data is not difficult, its reception and decoding require specific technologies. We present a 40 Gbps photoreceiver that exceeds the capabilities of current devices. This photoreceiver is based on a technology we call “nanodust.” This new technology enables nanoscale photodetectors to be embedded in matrices made from a different semiconductor, or directly integrated into a CMOS amplification circuit. Photoreceivers based on quantum dust technology can be designed to operate in any spectral region, including the telecommunications bands near 1.31 and 1.55 micrometers. This technology also lends itself to normal-incidence detection, enabling a large detector size with its associated increase in sensitivity, even at high speeds and reception wavelengths beyond the capability of silicon.

Keywords: 40 Gbps, Nanodust, Quantum Dot Photodetector, Si/Ge Photodetector, High Speed Photodetector, Monolithic Photoreceiver

1. Introduction

Most commercial integrated photoreceivers use silicon photodetectors. Complementary-metal-oxide-semiconductor (CMOS) monolithically integrated photoreceivers have been demonstrated to operate at 8 Gbps with 2 dBm (1.6 mW) average input optical power and a bit error rate of less than 10^{-9} , and are approaching 40 Gbps. However, these monolithic photoreceivers based on Si photodetector/amplifier integrated circuits have restricted spectral range that does not cover the 1.3 and 1.55 μm data communication bands¹⁻⁸.

To solve the problem of insensitivity of Si photoreceivers in the communication bands, several organizations are researching quantum-dot-array-based photodetectors. Ge/Si quantum dot photodetectors, for example, have been demonstrated in the laboratory to operate in the 1.3-1.55- μm spectrum⁹⁻¹². Fabrication for Si-based p-i-n photodiodes with a Ge quantum dot active layer operating in the 1300 nm – 1550 nm range has been reported¹¹. Several mature technologies are available for fabrication of such quantum-dot structures including molecular beam epitaxy (MBE)⁹, a subassembly electrochemical technique¹⁰, and fabrication of a Si/Ge quantum dot waveguide photodetector on silicon-on-insulator (SOI) substrate, growing the dot layer through a high-pressure chemical vapor deposition (HPCVD) process¹². In addition to these difficulties, an inherent problem with quantum dot based photoreceivers is their narrow band response, caused by energy level sharpening, a quantum effect. As a result, these photoreceivers have sensitivity at specific narrow wavelength bands within the 1.3-1.55 μm spectrum, thereby requiring several photoreceivers to cover the entire communications band.

Developing a complete photoreceiver with sufficient sensitivity and capability of handling the several tens of Gbps data rates requires integration of the photoreceiver and the amplifier monolithically in the same quantum dot layer. We demonstrated for the first time a nanodust photoreceiver with an integrated transimpedance amplifier. The photoreceiver covers the 1300 to 1550 nm telecommunication wavelength range, with data transfer at >40 Gbps, and will also receive RF-modulated signals at frequencies up to 40 GHz.

2. Sensor design and fabrication

Nanodust technology avoids narrow band quantum dot effects and has feature sizes much less than the wavelength of the light to be detected. This makes the device a broadband detector covering the entire 1.3-1.55 μm communications band. The unique design of the photoreceiver enables normal-incidence photodetection, resulting in an overall response characteristic that is virtually decoupled from the thickness of the active region – resulting in a large detector bandwidth.

Preliminary tests were performed on a quantum dot photodetector, fabricated as a 3-inch wafer (Fig 2-1). This wafer was laser-cut into pieces between 5 mm and 15 mm on a side, with the majority 10 mm \times 10 mm. These pieces were integrated into photoreceivers and tested.



Fig. 2-1. Preliminary photodetector wafer.

The preliminary (first generation) test photoreceiver was a 10 mm × 10 mm piece of the semiconductor wafer attached to a power supply and a resistor, with voltage across the resistor being the signal. In the second generation we fabricated a low-speed TIA from monolithic components. Operation at low frequency enabled use of a breadboard and long cables in the first generation tests, while higher frequency tests were performed on the second generation photoreceiver (Fig. 2-2).

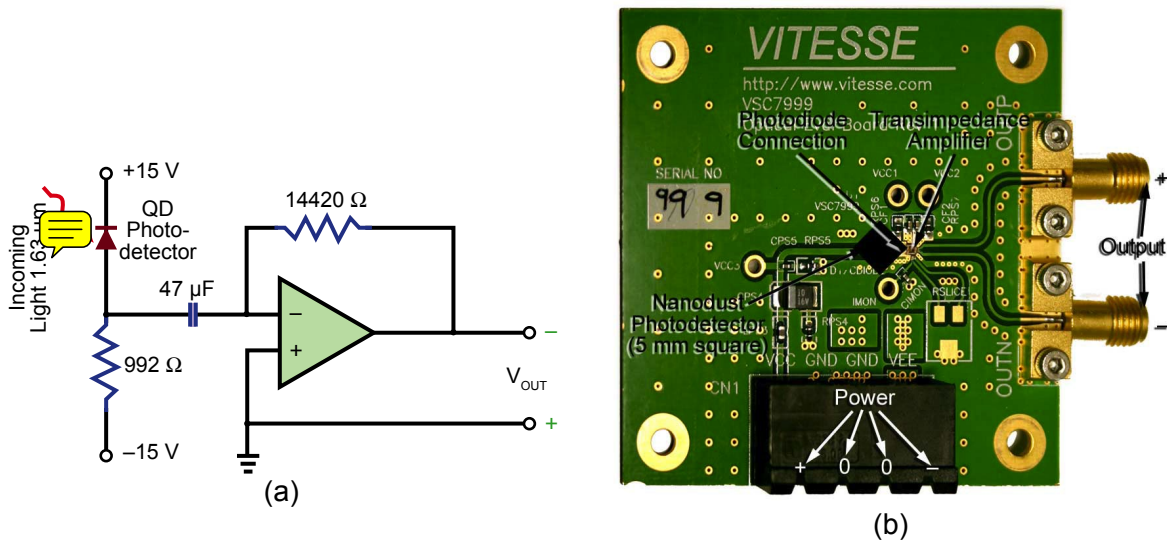


Figure 2-2

The first-generation nanodust photodetector was tested with a simple system in which the photocurrent served as input to a discrete-component TIA (a), while the second-generation system was integrated with a commercial TIA (b).

3. Measurements

To determine the potential carrier density, which depends on thermal generation rate, dark current, and carrier mobility, we measured the Hall mobility of the carriers. Thermal generation rate inside the quantum dots is assumed to be the same as in bulk material. Extensive characterization of the properties of similar Si/Ge quantum dot nanostructures was conducted to determine optimum nanostructure parameters.

3.1. Measurement of Hall Mobility

We measured the Hall mobility in a range of $\text{Ge}_x\text{Si}_{1-x}/\text{Si}$ quantum dot superlattices, with $x \in \{0, 0.50, 0.73\}$. In this experiment, the quantum dots were dome-shaped with base size ~ 40 nm and height ~ 4 nm. The density of quantum dots was $\sim 3 \times 10^9 \text{ cm}^{-2}$. (By comparison, the wafer we tested optically incorporated quantum dots of ~ 20 nm diameter and 1.12 nm thickness, with a density of $\sim 10^{11} \text{ cm}^{-2}$.)

Hall mobility in intrinsic Si is $\sim 1050 \text{ cm}^2/\text{V-s}$ at 300 K (room temperature), where the carrier density is $1.5 \times 10^{10} \text{ cm}^{-3}$. Intrinsic Ge demonstrates Hall mobility of $2000 \text{ cm}^2/\text{V-s}$ with carrier density of $2.4 \times 10^{13} \text{ cm}^{-3}$ at room temperature. Having measured mobility at one temperature, we can calculate mobility at another temperature from

$$\mu_H(T) = \mu_H(300 \text{ K}) \left[\frac{300 \text{ K}}{T} \right]^{3/2}, \quad (3-1)$$

where μ_H is the Hall mobility and T is the temperature. Calculated values for Hall mobility of intrinsic Si and Ge over a range of temperatures are shown in Fig. 3-1. Calculated values for the Hall mobilities of intrinsic Si and Ge at 77 K are 8,000 and 15,000 $\text{cm}^2/\text{V-s}$, respectively.

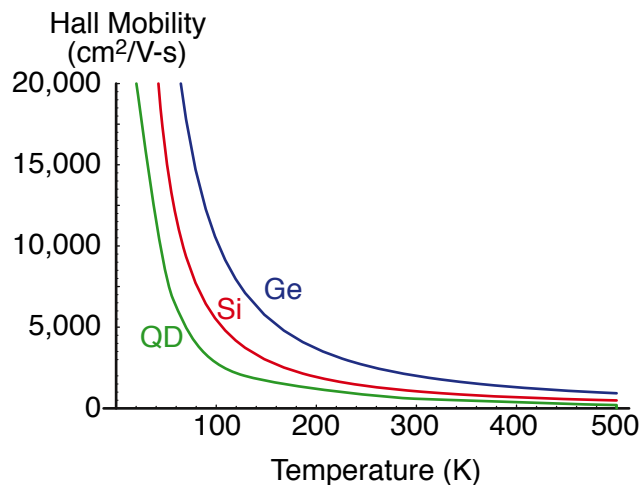


Figure 3-1

Calculated Hall mobility of intrinsic silicon (Si) and germanium (Ge), and measured Hall mobility in quantum dot region of tested superlattices (QD).

Hall mobility (μ_H) was measured for five Si/Ge quantum dot superlattices. Measurements varied from 228 cm²/V-s, with a five-layer structure having a carrier density of 1.76×10^{18} cm⁻³, to 239 cm²/V-s with a carrier density of 7.57×10^{18} cm⁻³ in a 20-layer structure. The relatively high Hall mobility and its T^{-3/2} dependence indicate that the carrier mobility of these quantum dot structures is based on electrons in the valence band, not hopping or trapped holes. The Hall mobility of these superlattices is nearly an order of magnitude greater than that expected in Si/Ge quantum well superlattices. Thus, the maximum operating frequency of a Si/Ge nanodust photodetector is expected to be much higher than that of a quantum well Si/Ge photodetector.

The Hall mobility is an important parameter because it can be used to calculate the speed at which carriers diffuse across the intrinsic region of the photodetector. The Hall mobility of a vertical section of our test sensor, together with the intrinsic electric field, is virtually infinite in the electrode/conductor regions, ~1050 cm²/V-s in the intrinsic Si regions, and ~230 in the active photodetection section. The intrinsic or applied electric field is several orders of magnitude greater in the active region than in any other. Since the intrinsic field is 2.4 V, any bias voltage will increase the field in these regions by the ratio of the bias voltage to this intrinsic field.

The intrinsic diffusion of 14.5 ps corresponds to a photovoltaic bandwidth of 125 GHz. With design optimization this bandwidth can be increased to >450 GHz.

3.2. Expected Absorptivity

The absorption spectrum of a single quantum dot layer is

$$\alpha(\lambda) = A \frac{n}{D} \frac{\sigma_{\text{QD}}}{\sigma_{\text{tot}}} \exp \left[- \frac{[hc(\lambda - \lambda_G)]^2}{(\lambda \lambda_G \sigma_{\text{tot}})^2} \right], \quad (3-2)$$

where α is absorption, A is peak absorption, n is the area density of free carriers in the ground state, D is the area density of dots, σ_{QD} and σ_{tot} are average Gaussian absorption linewidths for individual quantum dots and the ensemble of quantum dot respectively, λ is the wavelength of the incoming light, and $\lambda_G = hc/E_G$ is the center wavelength of the optical transition (the mean bandgap wavelength, which is ~1.55 μm for Ge).

3.3. Material capacitance

We also studied capacitance as a function of voltage and frequency at room temperature and thermal conductivity. Capacitance – voltage (CV) characteristics are important for integration of the photodetector with the receiver components and estimation of the operation speed. Thermal characteristics are also important since the excess heat removal is always an issue in downscaled integrated devices. Fig. 3-2 shows CV characteristics of the structure for frequency increasing from 50 kHz to 1 MHz. For the case of reverse bias (operating in photoconductive mode), the capacitance is approaching 150 pF/cm².

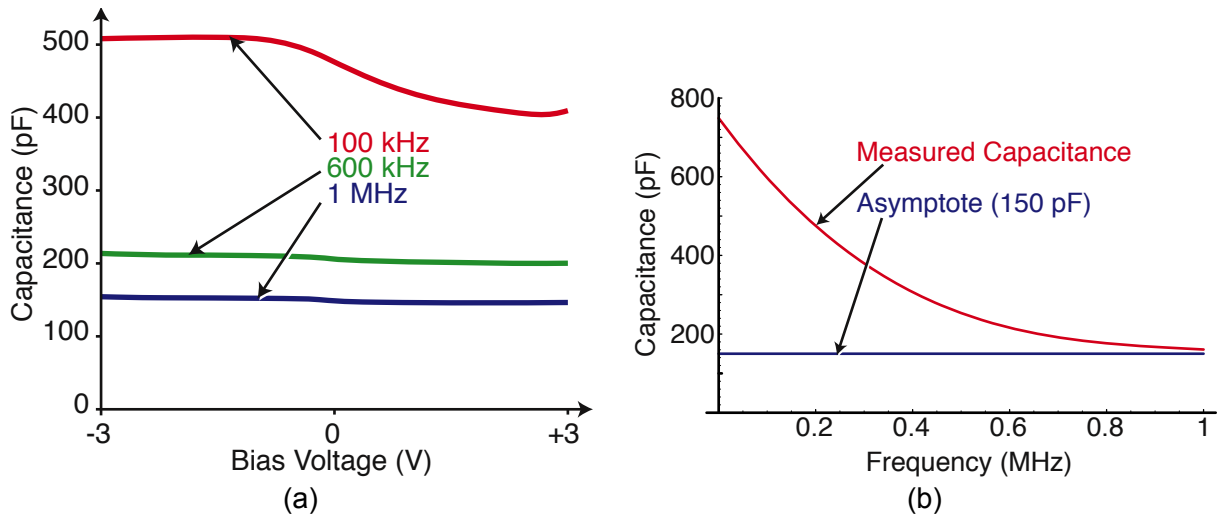


Figure 3-2
Capacitance-voltage characteristics of the Si/Ge nanodust photodetector.

The measured capacitance does not appear to vary significantly with temperature. From the high-frequency capacitance and size parameters of the nanodust material tested, we can calculate an effective dielectric permittivity of ~ 0.87 pF/m, or $\sim 0.095 \epsilon_0$. Given the typical TIA input impedance of 50Ω and the mobility measured in Section 3.1, we can estimate the cutoff frequency of our second-generation nanodust photoreceiver to be that shown in Fig. 3-3, based on 15 V reverse bias. The capacitance, not the diffusion speed, clearly, is the main effect limiting the cutoff frequency. The cutoff frequency can be increased by using a TIA with lower input impedance.

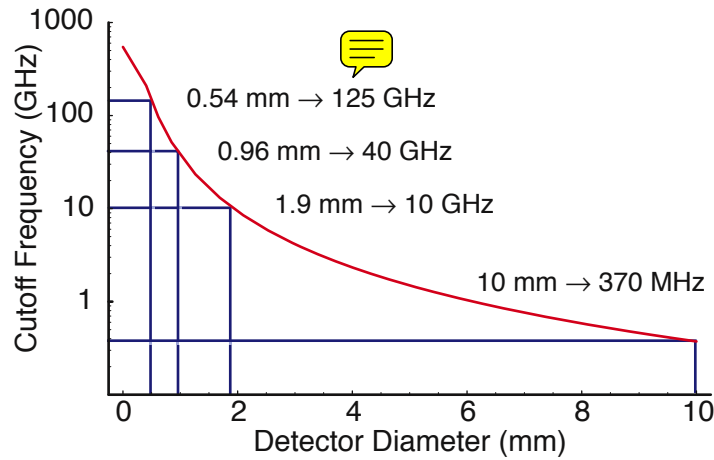


Figure 3-3
Capacitance limits the maximum frequency of the nanodust photoreceiver.

3.4. Si/Ge quantum dot photodetector thermal conductivity

Figure 3-4 shows cross-plane thermal conductivity of a prototype Ge/Si QDS structure, together with virtually identical structures using different quantum dot thicknesses. The results indicate significant decrease of the thermal conductivity compared to constituent bulk materials (thermal conductivity in pure bulk Si is 145 W/m-K while Ge bulk thermal conductivity is 59 W/m-K, both measured at ~300 K). The lower thermal conductivity in the quantum dot structure may lead to increased heat in that area. This effect must be considered in future nanodust detector designs.

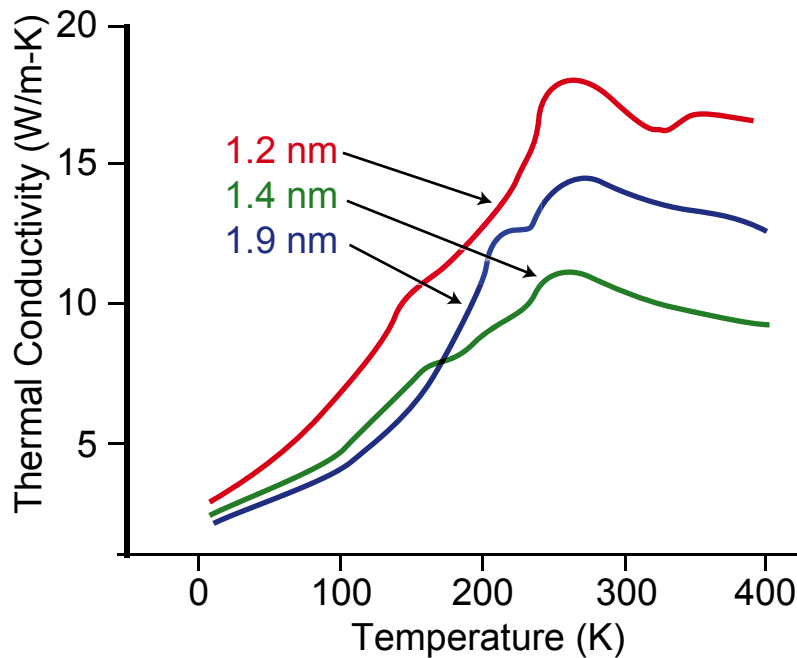


Figure 3-4
Thermal conductivity of Ge/Si quantum dot superlattice structures. In this graph, the asterisks represent a structure with 1.2-nm dots, the crosses 1.4 nm, and the x's 1.9 nm.

4. Electronic testing

We measured the overall responsivity and sensitivity of the Si/Ge quantum dot sensor with off the shelf instruments. Components of the device under test (DUT) are the wafer, a power supply, a transimpedance amplifier, and test equipment. The wafer was fabricated and cut to size, and the electrodes were wire bonded to the chip. The transimpedance amplifier evaluation board was ordered from Vitesse. To measure the responsivity of the photodiode, we mounted a 5 mm × 5 mm piece in the circuit shown in Figure 4-1.

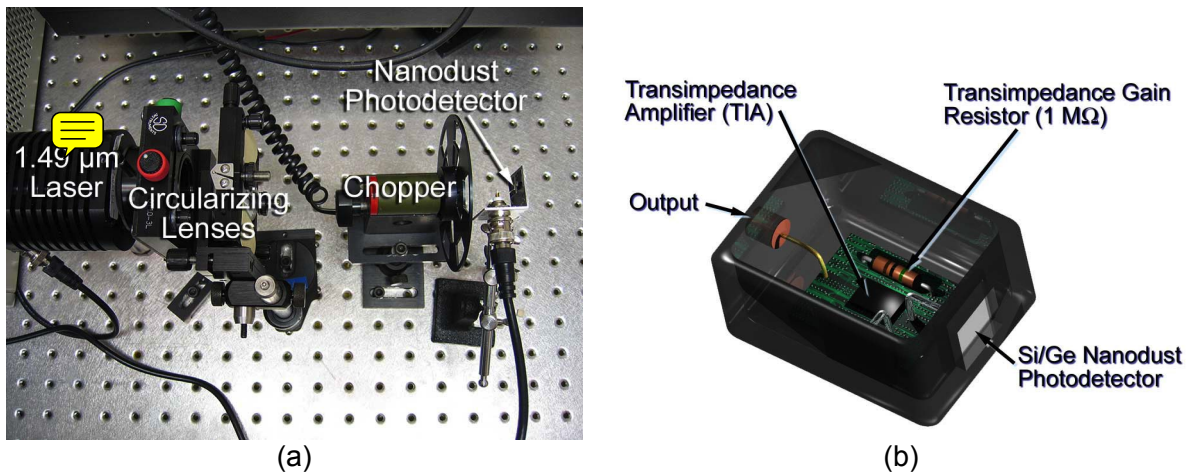


Figure 4-1

Testing the Si/Ge nanodust photodiode (a) required a transimpedance amplifier circuit (b).

4.1. Si/Ge nanodust responsivity

The testing system consisted of a laser diode operating at 1.49 μm , a pair of cylindrical lenses to circularize the beam, a chopper, the detector holder, and the TIA circuit shown in Figure 4-1 (b). The TIA used in these preliminary measurements had a gain of $\sim 14 \text{ mV}/\mu\text{A}$. Diode reverse bias was 9.6 V. Detector noise does not appear to change with frequency, averaging 0.2 A . Output measurements are shown in Figure 4-2.

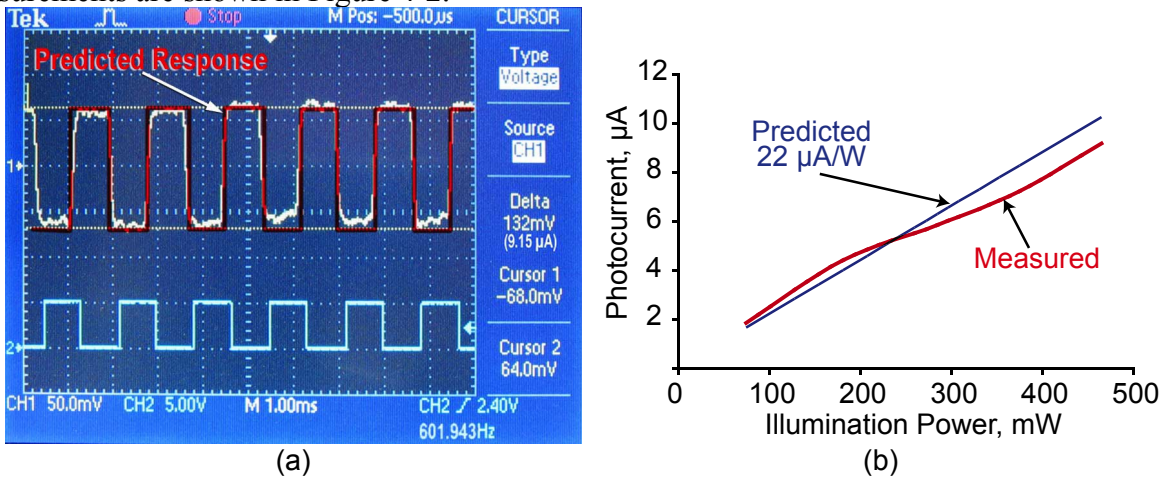


Figure 4-2

The response of the photodiode (a) is very close to the predicted 22 A/W at 1.49 μm (b).

4.2. Frequency Response

Fig. 4-3 shows the response of the Si/Ge nanodust photodetector with a 1 kHz directly modulated 1.49 μm laser. The photodetector response signal was amplified with a TIA as shown in Fig. 4-1 (b) and measured with a high-speed digital storage oscilloscope.

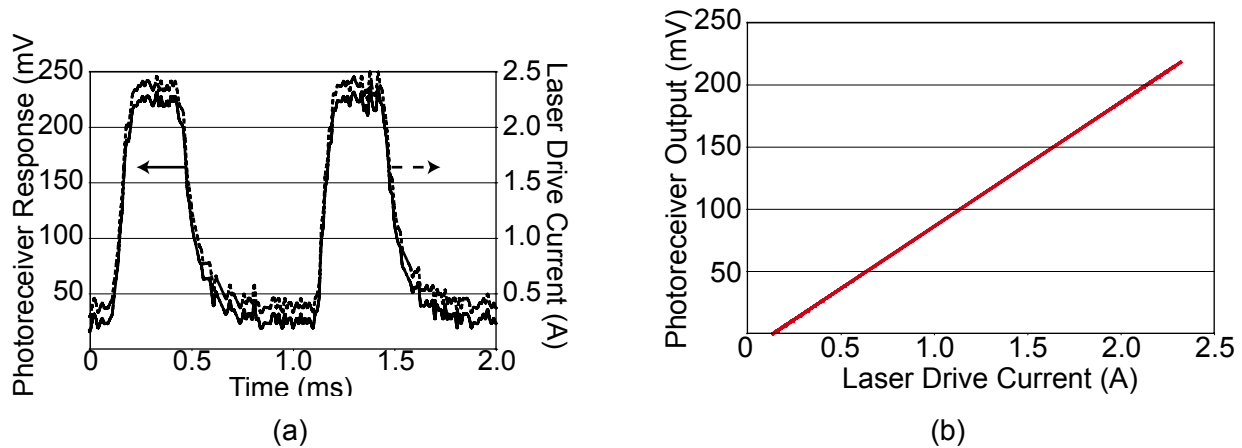


Figure 4-3

The Si/Ge nanodust integrated photoreceiver response at 1 kHz laser modulation (a) is virtually identical to the current itself, which represents the laser output. The measured response is nearly linear with a slope of 100 mV/A (b).

From Fig. 4-4, we observe that the photodetector tracks the laser modulation to an accuracy of at least 0.01ns. Based on this, the intrinsic responsivity of the photodetector is estimated to be greater than 100 GHz. This is significantly better than calculated for Eq. (3-5), indicating that the input impedance is lower than the estimated 50 Ω . We are in the process of building a high-speed photoreceiver test setup and new signal processing electronics to accurately determine the speed of this nanotechnology-based detector.

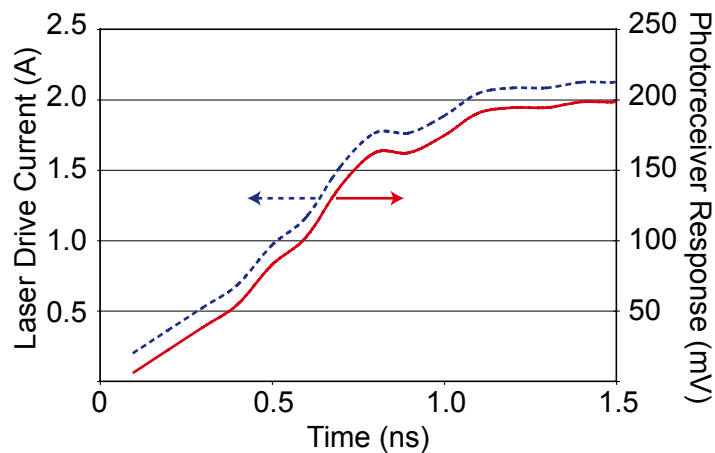


Figure 4-4

The photoreceiver response (solid line) accurately tracks the laser drive current (dashed line), even over very short time periods.

5. Conclusion

We have successfully demonstrated for the first time the feasibility of a novel monolithic nanodust/CMOS photoreceiver covering the 1300 to 1550 nm telecommunication wavelength range, with data transfer at ≥ 40 Gbps. Our data indicates that the photoreceiver has the potential of high sensitivity in the 1300 and 1550 nm communication bands, polarization insensitive operation at greater than 40 Gbps. A preliminary device was fabricated and characterized. This photodetector was extensively tested in the laboratory to ensure its quality and suitability for the photoreceiver. We assembled a first generation proof-of-concept prototype and successfully demonstrated its responsivity at a wavelength longer than the longest L-band telecommunication wavelength.

6. REFERENCES

1. D.H. Hartman, M.K. Grace, and C.R. Ryan, "A Monolithic Silicon Photodetector/Amplifier IC for Fiber and Integrated Optics Application," *J. Lightwave Tech.*, **3**, 729-738, 1985.
2. S.M. Csutak, J.D. Schaub, W.E. Wu, R. Shimer, and J.C. Campbell, "High-Speed Monolithically Integrated Silicon Photoreceivers Fabricated in 130-nm CMOS Technology," *J. Lightwave Tech.*, **20**, 1724-1729, 2002.
3. B. Yang, J.D. Schaub, S.M. Csutak, D.L. Rogers, and J.C. Campbell, "10-Gb/s All-Silicon Optical Receiver," *IEEE Phot. Tech. Lett.*, **15**, 745-747, 2003.
4. J.D. Schaub, R. Li, C.L. Schow, J.C. Campbell, G.W. Neudeck, and J. Denton, "Resonant-Cavity-Enhanced High-Speed Si Photodiode Grown by Epitaxial Lateral Overgrowth," *IEEE Phot. Tech. Lett.*, **11**, 1647-1649, 1999.
5. M.K. Emsley, O. Dosunmu, and Ünlü, "High-Speed Resonant-Cavity-Enhanced Silicon Photodetectors on Reflecting Silicon-On-Insulator Substrates," *IEEE Phot. Tech. Lett.*, **14**, 519-521, 2002.
6. T.K. Woodward and A.V. Krishnamoorthy, "1-Gbit/s CMOS Photoreceiver with Integrated Detector Operating at 850 nm," *Electronics Letters*, **34**, 1252-1253, 1998.
7. M.Y. Liu, E. Chen, and S.Y. Chou, "140-GHz Metal-Semiconductor-Metal Photodiodes on Silicon-on-Insulator Substrate With a Scaled Active Layer," *Appl. Phys. Lett.*, **65**, 887-888, 1994.
8. J.Y.L. Ho and K.S. Wong, "High-Speed and High-Sensitivity Silicon-on-Insulator Metal-Semiconductor-Metal Photodetector With Trench Structure," *Appl. Phys. Lett.*, **69**, 6-8, 1996.
9. J.L. Liu, W.G. Wu, A. Balandin, G.L. Jin, and K.L. Wang, "Intersubband Absorption in Boron-Doped Multiple Ge Quantum Dots," *Appl. Phys. Lett.*, **74**, 185-187, 1999.
10. A. Balandin, K.L. Wang, N. Kouklin, and S. Bandyopadhyay, "Raman Spectroscopy of Electrochemically Self-Assembled CdS Quantum Dots," *Appl. Phys. Lett.*, **76**, 137-139, 2000.
11. A.I. Yakimov, A.V. Dvurechenskii, A.I. Nikiforov, S.V. Chaikovskii, and S.A. Tiis, "Ge/Si Photodiodes with Embedded Arrays of Ge Quantum Dots for the Near Infrared (1.3-1.5 μm) Region," *Semiconductors*, **37**, 1345-1349, 2003.
12. J. Phillips, "Evaluation of the Fundamental Properties of Quantum Dot Infrared Detectors," *J. Appl. Phys.*, **91**, 4590-4594, 2002.
13. E.D. Palik, ed. *Handbook of Optical Constants of Solids*, Academic Press, New York, 1999.